Pergamon

Int. J. Heat Mass Transfer. Vol. 37, No. 7, pp. 1133–1142, 1994

0017-9310/94 $6.00 + 0.00

0017-9310(93)E0023-A

The temperature of fibers during air-gap wet-spinning: cooling by convection and evaporation

VOLKER SIMON†

Fachgebiet Technische Strömungslehre, Technische Hochschule Darmstadt, Petersenstr. 30, 64287 Darmstadt, FRG

(*Received* 20 *July* 1993 *and in final form* 25 *October* 1993)

Abstract—Fibers that are produced by air-gap wet-spinning are composed of cellulose, solvent and water. In the air-gap, the water evaporates at the fiber surface and this contributes to the cooling of the fiber. Here we determine the fiber temperature in the air-gap by taking into account heat conduction and convection as well as heat transfer due to evaporation. The computed temperature profiles are compared to experimental data. It is found that, close to the spinneret, water evaporates, enhancing the cooling of the fiber. At larger distances, water-vapour condenses at the fiber surface, lowering the cooling rate. The ultimate fiber temperature exceeds the temperature of the surrounding air and is determined by the balance between heat removal by convection and heat supply by condensation.

1. INTRODUCTION

AIR-GAP wet-spinning is a major commercial technique to produce synthetic fibers. In this process the spinning solution is extruded through a spinneret hole as a hot melt. The fiber is first drawn through an air-gap, where it is stretched and cooled, then it traverses the coagulation bath. Finally, the fiber is collected on a wind-up roll for further treatment. The process is shown schematically in Fig. 1.

The spinning solution is a ternary system, composed of cellulose, solvent and nonsolvent; the latter is usually water. Solidification of the fiber is brought about by diffusional exchange of solvent and nonsolvent in the coagulation bath. A brief description of the mechanics of the process has recently been given in ref. [1].

The fiber quality as well as the production rate are of prime importance to the manufacturer. The fiber quality is, of course, affected by the material itself, i.e. the molecular mass, composition and chemical structure of the cellulose and of the solvent. It also depends on the rate of solidification in the bath, and is thus influenced by bath temperature and composition. The quality is mainly influenced, however, by the rate of fiber stretching. Stretching aligns the molecules and thus leads to a high degree of orientation of the molecular chains. The orientation of the molecules, in turn, determines the strength and the mechanical properties of the fiber. It is therefore desirable, to produce fibers with an even and uniform stretch rate along the spinning line. The rate of stretching also affects the rate of fiber production and hence the efficiency of a given process.

The motion of the fiber, and in turn the rate of stretching, is primarily influenced by the material properties, i.e. its viscosity. Because the melt viscosity strongly depends on temperature, a detailed knowledge of the fiber temperature is indispensable in order to correctly predict the velocity of the fiber. Conversely, the fiber temperature can be an effective means of influencing and controlling the fiber velocity and thereby the entire spinning process. Therefore, determination of the fiber temperature in the spinning process is of great practical importance.

In this paper we examine the fiber temperature in the air-gap. The fiber temperature in the coagulation bath is not considered here, because this leads to a classic problem in heat conduction and its well known solution [2].

Much research has been devoted to the determination of the temperature profile of melt spun fibers. Bourne and Dixon [3], for example, used an integral method to solve the equations that govern

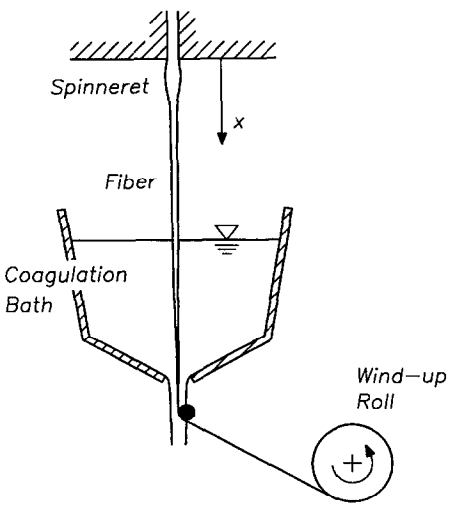

FIG. 1. Sketch of the spinning process.

†Present address: Stiftstr. 46, 45470 Mülheim/Ruhr, FRG.

NOMENCLATURE

a	fiber radius [m]
A	constant in equation (32)
$B_1 \ldots B_6$	parameters in equations (48)–(50)
c_p	specific heat at constant pressure [J kg^{-1} K^{-1}]
C	normalized concentration
D	binary diffusion coefficient [m^2 s^{-1}]
f	stream function
F	dimensionless saturation pressure
h	enthalpy [J kg^{-1}]
$h_n^V - h_n^L$	heat of evaporation [J kg^{-1}]
L	length of air-gap [m]
$\mathbf{n}$	unit normal vector
$\mathbf{m}_i$	mass flux of species i [kg m^{-2} s^{-1}]
M	molecular weight of mixture [kg mol^{-1}]
M_i	molecular weight of species i [kg mol^{-1}]
p_n	saturation pressure of component n in mixture [N m^{-2}]
$\tilde{p}_n$	saturation pressure of pure component n [N m^{-2}]
p_0	ambient pressure [N m^{-2}]
Pr	Prandtl-number, ν/κ
$\mathbf{q}$	heat flux [W m^{-2}]
$\mathbf{q}_f$	heat flux by conduction [W m^{-2}]
r	radial coordinate [m]
R_n^V	gas constant of component n [J kg^{-1} K^{-1}]
Sc	Schmidt-number, ν/D
T	temperature [K]
T_F	fiber temperature [K]
T_m	temperature at centerline of the fiber [K]
$\bar{T}$	mean temperature, $(T_0+T_\infty)/2$ [K]
$\mathbf{u}$	velocity [m s^{-1}]
u	axial velocity component [m s^{-1}]
U	fiber velocity [m s^{-1}]
v	radial velocity component [m s^{-1}]
$\dot{V}$	volume flow rate [m^3 s^{-1}]
w	mass fraction
x	axial coordinate [m]
X	axial coordinate
y_i	mole fraction
Y	radial coordinate.

Greek symbols

γ_n	activity coefficient
δ_D	thickness of concentration boundary layer [m]
δ_T	thickness of thermal boundary layer [m]
η	radial coordinate, $Y\sqrt{Pr}$
Θ	normalized temperature
κ	thermal diffusivity [m^2 s^{-1}]
λ	thermal conductivity [W m^{-1} K^{-1}]
ν	kinematic viscosity [m^2 s^{-1}]
ξ	axial coordinate, $X/\sqrt{Pr}$
ρ	mass density [kg m^{-3}]
φ	relative humidity
ψ	stream function [m^3 s^{-1}].

Subscripts

a	air
i	generic species
n	nonsolvent (water)
r	reference state
s	solvent
w	at the wall $r = a$
∞	at large distances
0	at the spinneret.

Superscripts

V	vapour
L	liquid.

conductive and convective heat transfer within the boundary layer generated by a moving fiber. Kuiken [4] has given analytic solutions for the temperature field by means of series expansions which are valid close to the orifice and far downstream. Because these series lacked an intermittent region of common validity, Münzing [5] solved the equations numerically. All of these results, however, failed to reproduce the experimental data for the fiber temperature that were measured during air-gap wet-spinning; the predicted values for the temperature were higher than those measured in the experiments.

This discrepancy can be resolved by observing that in air-gap wet-spinning the fibers contain water. Unlike in melt-spinning, the water may evaporate at the fiber surface and this contributes to the cooling of the fiber.

The saturation concentration of water-vapour at the fiber surface is imposed by the condition of thermodynamic equilibrium. The value of the concentration depends on ambient pressure, on water content within the fiber and, in particular, on the temperature of the fiber. At extrusion, the fiber temperature is rather high and the corresponding concentration of water-vapour at the fiber surface can exceed the value of concentration of water-vapour in the ambient air. As a result, a concentration gradient is established which leads to a mass flux of water-vapour from the fiber to the surrounding air. This mass flux is maintained by continuous evaporation of water at the fiber surface and the heat that is necessary to evaporate the water must be supplied by the fiber. This leads to a more rapid cooling than that in melt spinning.

Here we carry out an analysis of fiber cooling that includes cooling by conduction and convection as well as by evaporation of water at the fiber surface. In the analysis, it is assumed that the flow generated by the

moving fiber is steady and axisymmetric. Although the Reynolds number is large enough to justify the usual boundary layer assumptions, it is assumed to be small enough for the flow to be laminar. All physical properties are taken to be constant.

Air-gap wet-spinning is usually carried out under moderate ambient temperatures and pressures. Therefore, the solvent does not vaporize and the surrounding air is insoluble in the fiber. The fiber is, then, a ternary system composed of cellulose, solvent and water, while its environment is a binary mixture of water-vapour and air. It is further assumed that the condition of thermodynamic equilibrium at the phase boundary is unaffected by the presence of cellulose, which merely acts as an inert matrix.

Two additional simplifications are possible when modeling the air-gap wet-spinning process. First, because the change of concentration within the fiber and the change of the mass flux of the fiber due to evaporation are small, we will neglect them. Second, because the change of temperature over the cross-section of the fiber is small, we will assume that the fiber temperature varies only with distance from the spinneret. The estimates which lead to these simplifications, as well as the conditions which must be met if they are to be valid, are given in Section 2.

Despite all of these simplifications, the equations that govern the convective heat and mass transfer in the fiber and its surroundings have to be solved numerically. These equations, along with the relevant initial and boundary conditions, are provided in Section 3. Section 4 is devoted to the determination of the concentration of water-vapour at the fiber surface as imposed by thermodynamic equilibrium, and, in Section 5, a brief account is given of the numerical solution procedure. The computed temperature profiles are compared to experimental data in Section 6. The agreement is rather good and supports the proposed model. Our conclusions are presented in Section 7.

2. ESTIMATES AND SIMPLIFICATIONS

Before we establish the conditions that must be satisfied for the assumptions of constant concentration within the fiber and constant temperature over the cross-section of the fiber to be admissible, we introduce the measures of concentration that will be used and the necessary notation. For the time being, we restrict our analysis to a fiber of constant radius a which is drawn with constant speed U through an environment that is otherwise at rest. We later comment on the case of variable fiber velocity.

In the fiber, the cellulose acts as a matrix that is neither involved in the diffusion process nor does it influence thermodynamic equilibrium. Therefore, a suitable measure of concentration within the fiber must ignore the presence of cellulose [6], and the composition of the fiber may be specified through the mass fractions w_n^L and w_s^L with $w_n^L + w_s^L = 1$. Likewise, the composition of the environment of the fiber is specified through the mass fractions w_n^V and w_a^V with $w_n^V + w_a^V = 1$. Here, superscripts V and L are used to distinguish quantities in the vapour and the liquid state, and indices n, s and a refer to nonsolvent (i.e. water), solvent and air, respectively.

The initial values of fiber temperature and of mass fraction of water-vapour at the fiber surface are denoted by T_0 and w_{n0}^V, respectively, and the corresponding values at large distances from the fiber are given by T_∞ and $w_{n\infty}^V$. The concentration of water-vapour w_{nw}^V at the fiber surface is related to the water content within the fiber w_{nw}^L, to the ambient pressure p_0, and to the temperature T_w at $r = a$ by the condition for thermodynamic equilibrium:

$$w_{nw}^V = \mathrm{fn}(w_{nw}^L, p_0, T_0) \quad \text{at} \quad r = a. \tag{1}$$

The precise functional form for equilibrium will be given in Section 4.

Following Kuiken [7], we base the estimates for the radial change of concentration w and temperature T on the conditions of continuity of mass flux $\mathbf{m}_i$ of species i and of heat flux $\mathbf{q}$ through the fiber surface:

$$(\mathbf{m}_i^L \cdot \mathbf{n}) = (\mathbf{m}_i^V \cdot \mathbf{n}) \quad \text{at} \quad r = a, \tag{2}$$

and

$$(\mathbf{q}_f^L \cdot \mathbf{n}) = (\mathbf{q}_f^V \cdot \mathbf{n}) + \rho^V (\mathbf{u}^V \cdot \mathbf{n})(h_n^V - h_n^L) \quad \text{at} \quad r = a, \tag{3}$$

where $\mathbf{n}$ is the unit normal directed from the fiber to the ambient air, $\mathbf{q}_f = -\lambda \nabla T$ is the heat flux due to conduction, λ is the thermal conductivity, ρ is the mass density, $\mathbf{u}$ is the velocity of a material particle, and $(h_n^V - h_n^L)$ is the heat necessary for evaporation.

The mass flux of species i,

$$\mathbf{m}_i = w_i \rho \mathbf{u} - \rho D \nabla w_i, \tag{4}$$

is the sum of convectional and diffusional mass fluxes, and D is the binary diffusion coefficient. Because the air is insoluble in the fiber and solvent does not vaporize, the corresponding mass fluxes vanish at the surface and we obtain

$$(\mathbf{m}_a^V \cdot \mathbf{n}) = 0 \quad \text{and} \quad (\mathbf{m}_s^L \cdot \mathbf{n}) = 0 \quad \text{at} \quad r = a. \tag{5}$$

The only species that is transferred across the phase boundary at $r = a$ is water, either in the liquid or the vapour state. Therefore,

$$\rho^L (\mathbf{u}^L \cdot \mathbf{n}) = (\mathbf{m}_n^L \cdot \mathbf{n}) \quad \text{and} \quad \rho^V (\mathbf{u}^V \cdot \mathbf{n}) = (\mathbf{m}_n^V \cdot \mathbf{n}) \quad \text{at} \quad r = a. \tag{6}$$

Using equations (4) and (6) we obtain the mass fluxes as

$$\rho^V (\mathbf{u}^V \cdot \mathbf{n}) = -\frac{\rho^V D^V}{1 - w_{nw}^V} (\nabla w_n^V \cdot \mathbf{n}) \quad \text{at} \quad r = a, \tag{7}$$

and

$$\rho^{L}(\mathbf{u}^{L}\cdot\mathbf{n}) = -\frac{\rho^{L}D^{L}}{1-w^{L}_{nw}}(\nabla w^{L}_{n}\cdot\mathbf{n}) \quad \text{at} \quad r=a. \tag{8}$$

The overall mass balance is obtained by summing (2) over all components i, which yields

$$\rho^{V}(\mathbf{u}^{V}\cdot\mathbf{n}) = \rho^{L}(\mathbf{u}\cdot\mathbf{n}) \quad \text{at} \quad r=a. \tag{9}$$

Upon inserting (7) and (8) in (9) we get

$$\frac{\rho^{V}D^{V}}{1-w^{V}_{nw}}(\nabla w^{V}_{n}\cdot\mathbf{n}) = \frac{\rho^{L}D^{L}}{1-w^{L}_{nw}}(\nabla w^{L}_{n}\cdot\mathbf{n}) \quad \text{at} \quad r=a. \tag{10}$$

Now estimates are needed of the magnitude of the gradients of w^{L}_{n} and w^{V}_{n} appearing in equation (10). A concentration boundary layer will develop in the fiber and its surroundings. The thickness of this layer is of order $\delta_{D}(x) \sim \sqrt{(Dx/U)}$. Because $\sqrt{(D^{L}L/(Ua^{2}))} \ll 1$ in the wet-spinning process, the thickness of the boundary layer within the fiber is small compared to the radius of the fiber over the entire length of the air-gap. Consequently, the concentration at the fiber core will remain at the value w^{L}_{n0} with which the fiber left the spinneret. Equation (10) then yields the estimate

$$\frac{w^{L}_{n0}-w^{L}_{nw}}{w^{V}_{nw}-w^{V}_{n\infty}} = O\left(\frac{\rho^{V}}{\rho^{L}}\sqrt{\left(\frac{D^{V}}{D^{L}}\right)}\frac{1-w^{L}_{nw}}{1-w^{V}_{nw}}\right). \tag{11}$$

Because the term on the right hand side of (11) is small compared to one for typical spinning conditions, we may set $w^{L}_{nw} \simeq w^{L}_{n0}$. In other words: if

$$\frac{\rho^{V}}{\rho^{L}}\sqrt{\left(\frac{D^{V}}{D^{L}}\right)}\frac{1-w^{L}_{nw}}{1-w^{V}_{nw}} \ll 1, \tag{12}$$

it is admissible to neglect the change of concentration within the fiber in the air-gap.

Now we consider the continuity of the heat flux at the fiber surface, equation (3), and its relation to the radial change of temperature. Similar to the concentration boundary layer, a temperature boundary layer will be established in the fiber and its environment. The thickness of this layer is of order $\delta_{T}(x) \sim \sqrt{(\kappa x/U)}$, where $\kappa = \rho/(\lambda c_{p})$ is the thermal diffusivity and c_{p} is the specific heat at constant pressure. However, because $\sqrt{(\kappa^{L}L/(Ua^{2}))} > 1$ in the spinning process, the thickness of the temperature boundary layer within the fiber will soon be larger than the fiber radius a. Therefore, the temperature at the filament core will begin to drop to a value T_{m} below the extrusion temperature T_{0} at only a small distance behind the spinneret. Then, (3) and (7) provide the estimate

$$\frac{T_{m}-T_{w}}{T_{w}-T_{\infty}} = O\left(\frac{\lambda^{V}}{\lambda^{L}}\sqrt{\left(\frac{Ua^{2}}{\kappa^{V}L}\right)} + \sqrt{\left(\frac{Ua^{2}}{D^{V}L}\right)}\frac{\rho^{V}D^{V}}{\lambda^{L}}\frac{(h^{V}_{n}-h^{L}_{n})}{(T_{w}-T_{\infty})}\frac{w^{V}_{nw}-w^{V}_{n\infty}}{1-w^{V}_{nw}}\right). \tag{13}$$

Because both terms on the right hand side of (13)

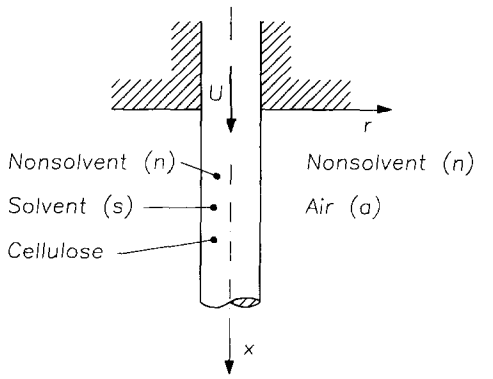

FIG. 2. Coordinate system and composition of the fiber.

are of equal magnitude and small compared to one for typical spinning conditions, we may set $T_{m} \simeq T_{w}$. If, therefore,

$$\frac{\lambda^{V}}{\lambda^{L}}\sqrt{\left(\frac{Ua^{2}}{\kappa^{V}L}\right)} \ll 1$$

and

$$\sqrt{\left(\frac{Ua^{2}}{D^{V}L}\right)}\frac{\rho^{V}D^{V}}{\lambda^{V}}\frac{(h^{V}_{n}-h^{L}_{n})}{(T_{w}-T_{\infty})}\frac{w^{V}_{nw}-w^{V}_{n\infty}}{1-w^{V}_{nw}} \ll 1, \tag{14}$$

it is admissible to neglect the change of temperature over the cross-section of the fiber.

3. BALANCE LAWS

We write the equations that govern the convective heat and mass transfer and the initial and boundary conditions that supplement them with respect to the polar coordinate system shown in Fig. 2. The axial and radial velocity components are denoted by u and v, respectively. Applying the usual boundary layer approximations (see, e.g., [8]), the equations of motion and the equations for heat and mass transfer in the environment of the fiber are

$$\frac{\partial}{\partial x}(ru)+\frac{\partial}{\partial r}(rv) = 0, \tag{15}$$

$$u\frac{\partial u}{\partial x}+v\frac{\partial u}{\partial r} = \frac{v}{r}\frac{\partial}{\partial r}\left(r\frac{\partial u}{\partial r}\right), \tag{16}$$

$$u\frac{\partial T}{\partial x}+v\frac{\partial T}{\partial r} = \frac{\kappa^{V}}{r}\frac{\partial}{\partial r}\left(r\frac{\partial T}{\partial r}\right), \tag{17}$$

and

$$u\frac{\partial w^{V}_{n}}{\partial x}+v\frac{\partial w^{V}_{n}}{\partial r} = \frac{D^{V}}{r}\frac{\partial}{\partial r}\left(r\frac{\partial w^{V}_{n}}{\partial r}\right). \tag{18}$$

The mass of species and the overall mass of the fiber are conserved on account of the approximation $w^{L}_{n} \simeq \text{const.}$

An integral energy balance for the fiber gives

$$\rho^{L} U a^2 \pi c_p^{L} \frac{dT_F}{dx} = -2\pi a(\mathbf{q}_f^{L} \cdot \mathbf{n}), \tag{19}$$

where we have neglected axial heat conduction, T_F denotes the fiber temperature, and $(\mathbf{q}_f \cdot \mathbf{n})$ is the heat flux through the fiber surface. By use of (3) and (7) this heat flux may be written as

$$(\mathbf{q}_f^{L} \cdot \mathbf{n}) = -\lambda^{V} \frac{\partial T}{\partial r} - \frac{\rho^{V} D^{V}}{1 - w_n^{V}} \frac{\partial w_n^{V}}{\partial r} (h_n^{V} - h_n^{L}) \quad \text{at} \quad r = a. \tag{20}$$

Inserting this expression into (19) leads to

$$\rho^{L} U a c_p^{L} \frac{dT_F}{dx} = 2\lambda^{V} \frac{\partial T(a)}{\partial r} + 2 \frac{\rho^{V} D^{V}}{1 - w_n^{V}(a)} \frac{\partial w_n^{V}(a)}{\partial r} (h_n^{V} - h_n^{L}). \tag{21}$$

The equations (15)–(18) and (21) are supplemented by the initial and boundary conditions

$$u = U, \quad v = 0, \quad T = T_F = T_0, \quad w_n^{V} = \mathrm{fn}(w_{n0}^{L}, p_0, T_0) \quad \text{at} \quad x = 0, \quad r = a, \tag{22}$$

$$u = 0, \quad T = T_\infty, \quad w_n^{V} = w_{n\infty}^{V}, \quad \text{at} \quad x = 0, \quad r > a, \tag{23}$$

$$u = U, \quad v = 0, \quad T = T_F, \quad w_n^{V} = \mathrm{fn}(w_{n0}^{L}, p_0, T_F), \quad \text{at} \quad x \geqslant 0, \quad r = a, \tag{24}$$

and

$$u = 0, \quad T = T_\infty, \quad w_n^{V} = w_{n\infty}^{V} \quad \text{at} \quad x \geqslant 0, \quad r \to \infty. \tag{25}$$

Note that equations (17), (18) and (21) for species and energy conservation are nonlinearly coupled through the boundary conditions (22) and (24), and through the gradients of T and w_n^{V} that appear in (21).

According to the energy balance for the fiber, equation (21), the fiber temperature will change in response to a conductive heat transfer or a convective enthalpy transport through the fiber surface. Depending on the values of T_0, T_∞, w_{n0}^{V} and $w_{n\infty}^{V}$, the sign of the conductive heat flux $\mathbf{q}_f^{V} \cdot \mathbf{n} = \lambda^{V} \partial T / \partial r$ and of the convective enthalpy transport

$$\rho^{V}(\mathbf{u} \cdot \mathbf{n})(h_n^{V} - h_n^{L}) = -\rho^{V} D^{V} / (1 - w_n^{V}(a)) \partial w_n^{V}(a) / \partial r (h_n^{V} - h_n^{L})$$

may be either negative or positive and thus lead to either cooling or heating of the fiber. In most practical applications, T_0 will be greater than T_∞, and w_{n0}^{V} will be greater than $w_{n\infty}^{V}$. Consequently, the driving temperature and concentration differences $(T_F - T_\infty)$ and $(w_{nw}^{V} - w_{n\infty}^{V})$ will be greater than zero. In this case, both terms on the right hand side of (21) will have the same sign and both will contribute to the cooling of the fiber.

However, with increasing distance from the spinneret, the fiber temperature will decrease. With decreasing temperature, the value of w_{nw}^{V} will also decrease. Eventually, w_{nw}^{V} will be less than $w_{n\infty}^{V}$, and the mass flux of water-vapour will be directed from the environment to the fiber and water-vapour will condense at the fiber surface. As a result of this condensation, heat will be released and transferred to the fiber. In this case, the terms on the right hand side of (21) will have opposite signs: the first term will lead to cooling of the fiber due to heat conduction, and the second term will lead to heating of the fiber due to condensation of water-vapour at the fiber surface.

The temperature of the fiber ceases to change when the heat which is supplied by condensation equals the heat which is withdrawn by conduction and convection. Because heat is transferred to the fiber by condensation, the ultimate fiber temperature will be higher than the ambient temperature.

4. THERMODYNAMIC EQUILIBRIUM

As mentioned earlier, the concentration of water-vapour at the fiber surface is imposed by the condition of thermodynamic equilibrium. This condition provides a relation between pressure p, temperature T and concentrations w_i^{V} and w_i^{L} at the phase boundary. The concentrations are usually expressed in terms of mole fractions y_i, which are related to mass fractions w_i by

$$y_i = \frac{M}{M_i} w_i. \tag{26}$$

Here M_i is the molecular weight of the ith component and $M = \sum y_i M_i = 1/(\sum w_i / M_i)$ is the mean molecular weight of the mixture.

According to Gibbs' phase rule, a two-phase ternary system possesses three degrees of freedom. In the present context, these are given by the pressure p_0, temperature T_F and concentration of water y_n^{L} in the fiber. Following boundary layer theory, the pressure is constant over the boundary layer and is equal to the ambient pressure p_0; the initial values of temperature and concentration within the fiber are given at the exit of the spinneret, and their evolution in the air-gap is determined by the balance laws given in the last section. Therefore, the unknown quantities are y_a^{V}, y_a^{L}, y_s^{V}, y_s^{L} and y_n^{V}.

As was pointed out in the introduction, the air is insoluble in the fiber ($y_a^{L} = 0$), and the solvent does not vaporize ($y_s^{V} = 0$) at low temperatures and pressures. The remaining quantities are then determined by the two compatibility conditions

$$y_a^{V} = 1 - y_n^{V} \quad \text{and} \quad y_s^{L} = 1 - y_n^{L}, \tag{27}$$

and a thermodynamic equilibrium condition which relates y_n^{V} to y_n^{L}, p_0 and T_F. Following [9], this relation may be put in the form

$$y_n^{V} = \gamma_n(y_n^{L}) y_n^{L} \tilde{p}_n / p_0, \tag{28}$$

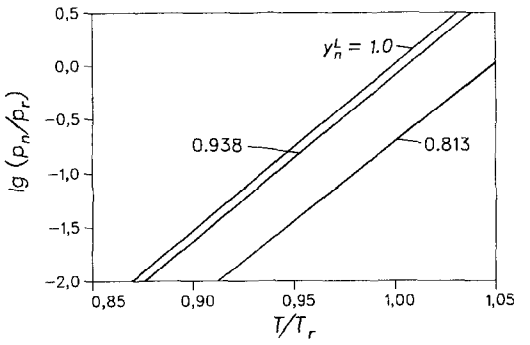

FIG. 3. Measured saturation pressures for a mixture of solvent and nonsolvent at various nonsolvent concentrations.

where $\gamma_n(y_n^L)$ is the activity coefficient and $\tilde{p}_n$ is the saturation pressure of the pure component n. We take $\tilde{p}_n$ to be given by the Clausius–Clapeyron equation,

$$\tilde{p}_n = p_r \exp\left(\frac{(h_n^V - h_n^L)}{R_n^V T_r}\left(1 - \frac{T_r}{T}\right)\right). \tag{29}$$

In this expression, p_r and T_r denote quantities at a reference state and R_n^V is the gas constant of the component n.

The activity coefficient is unknown, and the remainder of this section is devoted to its determination. To this end, we first determine γ_n for various values of water concentration w_n^L; we then seek an analytic expression to interpolate these data.

By virtue of Dalton's law the mole fraction at saturation is given by the ratio of partial to total pressure,

$$y_n^V = p_n(T, y_n^L)/p_0. \tag{30}$$

From equations (28) and (30) we obtain

$$\gamma_n = \frac{p_n(T, y_n^L)}{y_n^L \tilde{p}_n(T)}. \tag{31}$$

The data for the saturation pressure p_n as a function of temperature and concentration were supplied by the manufacturer of the fibers and are shown in Fig. 3. These data, together with equation (31), determine the experimental values of $\gamma_n(y_n^L)$, which are shown in Fig. 4.

A wealth of analytic expressions has been suggested

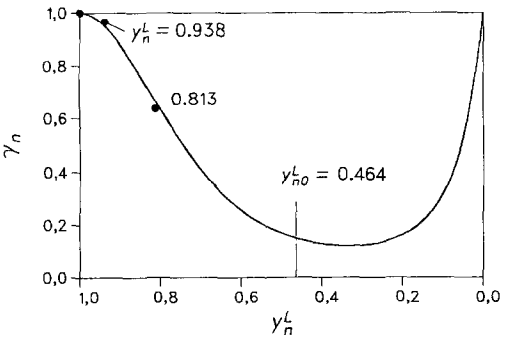

FIG. 4. Measured values (symbols) and analytic function for the activity coefficient.

in the literature (e.g. [9, 10]) to estimate activity coefficients. These expressions are based on excess functions and offer a thermodynamically consistent method to interpolate and extrapolate thermodynamic data. Here, we adopt the simplest expression for unsymmetric binary mixtures [9]:

$$\ln \gamma_n = 4A(1 - y_n^L)^2 y_n^L. \tag{32}$$

The constant A is chosen such that equation (32) interpolates the data for γ_n well; this yields $A = -3.56$. The corresponding curve is shown in Fig. 4.

In Section 6, computed temperature profiles are compared with experimental data. Unfortunately, however, the experimental data for the fiber temperature were obtained by spinning a solution with concentration $y_n^L = 0.464$. Therefore, equation (32) has to be used to extrapolate the corresponding value of γ_n and we obtain $\gamma_n(0.464) = 0.15$ (see Fig. 4).

For further convenience, we rewrite equation (28) with the aid of (26) and (29) to obtain

$$w_n^V(T) = w_{n0}^V \exp\left(\frac{(h_n^V - h_n^L)}{R_n^V T_0}\left(1 - \frac{T_0}{T}\right)\right), \tag{33}$$

where

$$w_{n0}^V = w_{n0}^L \gamma_n(w_{n0}^L) \frac{M^L}{M^V} \frac{p_r}{p_0} \exp\left(\frac{(h_n^V - h_n^L)}{R_n^V T_r}\left(1 - \frac{T_r}{T_0}\right)\right) \tag{34}$$

is the initial concentration at temperature T_0.

5. NUMERICAL SOLUTION

The system of equations (15)–(18) and (21) describes the evolution of five unknown quantities: u, v, T, T_F and w_n^V. The number of unknowns may be reduced to four by introducing a streamfunction ψ such that $\partial\psi/\partial r = ur$ and $\partial\psi/\partial x = -vr$. Equation (15) is then satisfied identically. A further reduction of the number of unknowns can be accomplished by exploiting the condition $T = T_F$ at $r = a$, and regarding the energy balance for the fiber, equation (21), as an additional boundary condition for the temperature field in the air-gap. In other words: ψ, T and w_n^V are taken to be the three primary unknowns, and after their determination the fiber temperature T_F is obtained upon evaluating T at $r = a$.

The numerical solution of the equations is carried out by using dimensionless quantities. Following Crane [11], we introduce the variables

$$X = \sqrt{\left(\frac{8vx}{Ua^2}\right)}, \quad Y = \frac{r^2 - a^2}{a^2}\sqrt{\left(\frac{Ua^2}{8vx}\right)},$$

$$\text{and} \quad f(X, Y) = \frac{1}{X}\frac{2\psi}{Ua^2}. \tag{35}$$

We further define

$$\Theta = \frac{T - T_\infty}{T_0 - T_\infty} \quad \text{and} \quad C = \frac{w_n^V - w_{n\infty}^V}{w_{n0}^V - w_{n\infty}^V}, \tag{36}$$

and cast equations (15) to (18) into the forms

$$\frac{\partial}{\partial Y}\left((1+YX)\frac{\partial^2 f}{\partial Y^2}\right) = -f\frac{\partial^2 f}{\partial Y^2} + X\left(\frac{\partial f}{\partial Y}\frac{\partial^2 f}{\partial X \partial Y} - \frac{\partial^2 f}{\partial Y^2}\frac{\partial f}{\partial X}\right), \tag{37}$$

$$\frac{\partial}{\partial Y}\left((1+YX)\frac{\partial \Theta}{\partial Y}\right) = -Pr\frac{\partial \Theta}{\partial Y}f + Pr\,X\left(\frac{\partial f}{\partial Y}\frac{\partial \Theta}{\partial X} - \frac{\partial f}{\partial X}\frac{\partial \Theta}{\partial Y}\right), \tag{38}$$

and

$$\frac{\partial}{\partial Y}\left((1+YX)\frac{\partial C}{\partial Y}\right) = -Sc\frac{\partial C}{\partial Y}f + Sc\,X\left(\frac{\partial f}{\partial Y}\frac{\partial C}{\partial X} - \frac{\partial f}{\partial X}\frac{\partial C}{\partial Y}\right). \tag{39}$$

The initial conditions (22) and (23) transform to

$$f = 0, \quad \frac{\partial f}{\partial Y} = 1, \quad \Theta = 1, \quad C = 1 \quad \text{at} \quad X = 0, Y = 0, \tag{40}$$

and

$$\frac{\partial f}{\partial Y} = 0, \quad \Theta = 0, \quad C = 0 \quad \text{at} \quad X = 0, Y \to \infty. \tag{41}$$

The boundary conditions (21), (24) and (25) become

$$f = 0, \quad \frac{\partial f}{\partial Y} = 1, \tag{42}$$

$$\frac{d\Theta}{dX} = \frac{B_1}{Pr}\left(\frac{\partial \Theta}{\partial Y} + \frac{Pr\,B_2}{Sc(B_3 - C)}\frac{\partial C}{\partial Y}\right), \tag{43}$$

and

$$C = F(\Theta) + B_4(F(\Theta) - 1) \quad \text{at} \quad X > 0, Y = 0, \tag{44}$$

and

$$\frac{\partial f}{\partial Y} = 0, \quad \Theta = 0, \quad C = 0 \quad \text{at} \quad X > 0, Y \to \infty, \tag{45}$$

where the function $F(\Theta)$ is given by

$$F(\Theta) = \exp\left(\frac{(h_n^V - h_n^L)}{R_n^V T_0}\left(1 - \frac{T_0}{T}\right)\right) = \exp\left(\frac{B_6(\Theta - 1)}{\Theta + B_5}\right). \tag{46}$$

The dimensionless parameters are

$$Pr = \left(\frac{\nu}{\kappa}\right)^V, \quad Sc = \left(\frac{\nu}{D}\right)^V, \tag{47}$$

$$B_1 = \frac{(\rho c_p)^V}{(\rho c_p)^L}, \quad B_2 = \frac{(h_n^V - h_n^L)}{c_p^V(T_0 - T_\infty^V)}, \tag{48}$$

$$B_3 = \frac{1 - w_{n\infty}^V}{w_{n0}^V - w_{n\infty}^V}, \quad B_4 = \frac{w_{n\infty}^V}{w_{n0}^V - w_{n\infty}^V}, \tag{49}$$

$$B_5 = \frac{T_\infty^V}{T_0 - T_\infty^V} \quad \text{and} \quad B_6 = \frac{(h_n^V - h_n^L)}{R_n^V T_0}. \tag{50}$$

The concentration of water-vapour at large distances is usually specified by prescribing the relative humidity $\varphi_n = p_n/\tilde{p}_n$. This leads to

$$w_{n\infty}^V = \varphi_{n\infty}\frac{M_n^V}{M^V}\frac{\tilde{p}_n(T_\infty)}{p_0}. \tag{51}$$

The momentum equation (37) is decoupled from the equations (38) and (39) and can be solved independently. Once $f(X, Y)$ is known, the equations (38) and (39) can be solved for $\Theta(X, Y)$ and $C(X, Y)$.

We note that X and Y are suitable measures of nondimensional distance for the temperature and concentration fields only if the Prandtl and Schmidt numbers are of order unity. If, for example, $Pr \gg 1$, better suited variables for the solution of (38) are $\xi = X/\sqrt{Pr}$ and $\eta = Y\sqrt{Pr}$.

The numerical scheme which has been chosen to solve the equations is due to Herring and Mellor [12]. The method consists of essentially two steps. In the first step, the equations are discretized in the X-direction according to the Crank–Nicholson scheme. In the second step, the resulting ordinary differential equations are solved with a Runge–Kutta method at a fixed value of X. The initial, similarity-type profiles are naturally obtained as solutions to the equations (37) to (39) upon setting X equal to zero.

The coupling between the equations (38) and (39) through the conditions (43) and (44) necessitates an iterative solution procedure. In an inner loop, we determine the temperature profile and solve equation (38) subject to the boundary conditions (43) and (45b) with prescribed values for C and $\partial C/\partial Y$ at $Y = 0$. In the outer loop, we determine the concentration profile and solve equation (39) with the boundary conditions (44) and (45c). This procedure is easily implemented and takes approximately nine iterations at each X-position to yield an upper relative error of 10^{-6} for the values and gradients of temperature and concentration at the fiber surface.

If we allow the fiber velocity to vary with distance from the spinneret, the equations (35), (36) and (38)–(46) remain unchanged, provided that $Ua^2 = \text{const}$. The changing fiber velocity makes itself felt only through the term $-2X(da/dX)(\partial f/\partial Y)^2$, which has to be added to the right hand side of (37). Münzing [5] has investigated the case of a fiber velocity varying linearly with x. He found that for typical spinning conditions the friction coefficient of a stretching fiber differs by at most 8% from the corresponding value obtained for constant U, while the fiber temperature

Table 1. Dimensionless parameters for temperature profiles; cases (i)–(v)

	i	ii	iii	iv	v
Pr	0.7	0.7	0.7	0.7	0.7
Sc	0.61	0.61	0.61	0.61	0.61
B_1	4.196E−04	4.196E−04	4.196E−04	4.196E−04	4.196E−04
B_2	30.77	41.96	24.29	24.29	41.96
B_3	31.35	115.5	13.40	24.94	121.4
B_4	0.369	1.360	0.157	0.080	4.431
B_5	3.973	5.418	3.137	2.926	5.782
B_6	13.41	14.17	12.37	13.41	13.41

is virtually unaffected. Therefore, we restrict our analysis to the case U = const.

6. RESULTS AND DISCUSSION

We now compare the model predictions to experimental data. The data for the fiber temperature were obtained in four different experimental set-ups, denoted by *I*.1 to *I*.4. Unfortunately, neither the temperature T_∞ nor the concentration $w^V_{n\infty}$ were measured at large distances from the fiber. Because the experiments were carried out under ordinary laboratory conditions, we assume that $T_\infty = 25°C$, and that the relative humidity was given by $\varphi_{n\infty} = 0.6$ in all set-ups.

The experimental set-ups differ in initial temperature T_0 and volume flow rate $\dot{V} = \pi U a^2$, all other parameters are the same. The difference in initial temperature is so slight (less than 4% at most) that we have used a mean value for comparison with the numerical computation. Note that the difference in volume flow rate merely shifts the experimental data along the dimensionless X-axis.

All physical properties were assigned values at a temperature $\bar{T} = (T_0 + T_\infty)/2$. The resulting combination of dimensionless parameters is denoted as case (i) and the values of Pr, Sc and B_1 to B_6 are collected in Table 1. The ratios of the volume flow rates in the experimental set-ups are given in Table 2. Details of the calculation procedure may be found in ref. [13].

Table 2. Ratios of volume flow rates

	I.1	*I*.2	*I*.3	*I*.4
$\dot{V}/\dot{V}_{I.1}$	1.000	0.206	2.794	0.353

The experimental data and computed temperature profiles with and without mass transfer are shown in Fig. 5. The agreement between the calculated profile which accounts for mass transfer and the measurements is fairly good and supports the proposed model. The vertical chain-dotted line in Fig. 5 indicates the distance from the spinneret at which the mass flux of water-vapour is reversed. For smaller distances water evaporates, and for larger distances water-vapour condenses at the fiber surface.

The temperature profile is governed by the dimensionless parameters Pr, Sc and B_1 to B_6. It would, of course, be possible to study the influence of these parameters by varying only one of them while keeping the others fixed. It is not obvious, however, how this variation could be achieved in practice. The only quantities that can be changed and controlled easily under industrial conditions are the initial and the ambient temperature. Due to their physical significance, these quantities appear in five dimensionless products, either directly, as in B_2, B_5 and B_6; or indirectly, as in B_3 and B_4 through w^V_{n0} and $w^V_{n\infty}$, which are related to T_0 and T_∞ through equations of state. Here, we choose to study the influence of the initial and the ambient temperature by assigning a few typical values for T_0 and T_∞ and express the values of the parameters in form of the dimensionless groups B_1 to B_6.

We study five cases, denoted by (i)–(v). Case (i) is given by the experimental conditions as explained above. In cases (ii) and (iii) we vary T_0, while in cases (iv) and (v) we vary T_∞. In case (ii), the initial temperature T_0 was chosen to be 20 K lower than in case (i), in case (iii) the temperature T_0 was chosen to be 20 K higher than in case (i).

In case (iv), the initial temperature was the same as in case (i) and the temperature T_∞ was chosen to be 20 K lower than in case (i), whereas in case (v) the temperature T_∞ was chosen to be 20 K higher than in case (i). The relevant parameters are tabulated in Table 1.

The temperature profiles for the cases (ii)–(v) are plotted in Figs. 6 and 7. The results can be explained by noting that an increase in initial temperature gives rise to an increase of the concentration of water-vapour at the fiber surface. Accordingly, the mass flux of water-vapour and the cooling-rate are larger and the fiber temperature falls off more quickly. Also, the distance over which water evaporates is longer and the final fiber temperature is lower relative to a case with low initial temperature.

Raising the temperature in the environment leads to a higher concentration $w^V_{n\infty}$ at infinity. The mass flux of water-vapour then diminishes and the location where condensation first occurs moves closer to the spinneret. Also, the final fiber temperature is lower,

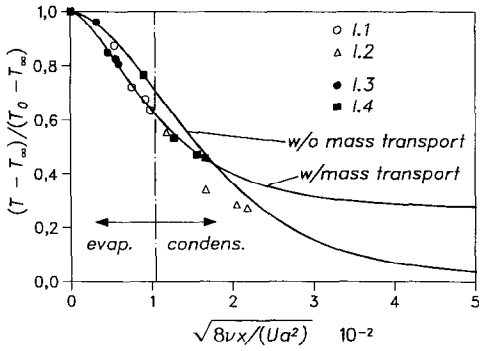

FIG. 5. Measured (symbols) and calculated (solid lines) fiber temperature with and without mass transfer; case (i). The vertical chain-dotted line denotes the distance at which the mass-flux of water-vapour is reversed. For smaller distances, water evaporates (denoted by evap), for larger distances water-vapour condenses on the fiber (denoted by condens).

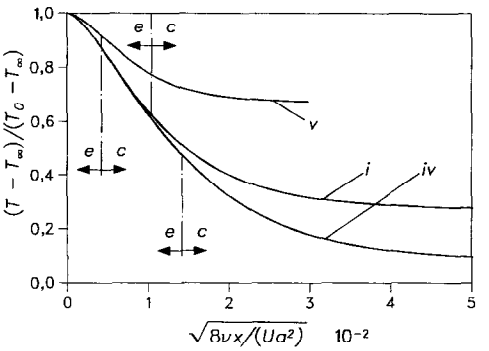

FIG. 7. Calculated temperature profiles for different ambient temperatures T_∞; cases (i), (iv) and (v). In case (iv), $T_{\infty,iv} = T_{\infty,i} - 20$ K. In case (v), $T_{\infty,v} = T_{\infty,i} + 20$ K.

because both driving differences $(T_0 - T_\infty)$ and $(w^V_{n0} - w^V_{n\infty})$ are smaller.

If the ambient temperature is high enough or if the initial temperature is low enough, the concentrations of water-vapour at the fiber surface and at large distances may be such that water-vapour begins to condense right at the spinneret.

7. CONCLUSIONS

A model has been presented for coupled heat and mass transfer that is applicable to fiber cooling in the air-gap wet-spinning process. It is shown that cooling in this process is markedly influenced by evaporation of the water which is contained within the fiber. The model predictions agree well with experiments and it is found that, in general, the water evaporates close to the spinneret, while for larger distances water-vapour condenses at the fiber surface. The ultimate fiber temperature is determined by a balance between cooling by convection and heating by condensation.

It is important to control the cooling of the fiber and the length along which water evaporates in the spinning process. This may be done by changing, for example, the temperature with which the fiber leaves the spinneret or the conditions in the ambient air. Neither change is unrestricted, however, since for large initial temperatures the spinning solution degrades, and complete control of the environment necessitates expensive air conditioning.

Excessive condensation of water-vapour at the fiber surface may have a negative impact on the spinning process, because the composition of the fiber changes due to evaporation and condensation. Even though it has been shown that the effect of changing concentration within the fiber on the fiber temperature is negligible, the effect on the mechanical properties of the fiber may be appreciable, because the spinning solution solidifies instantaneously when the solvent concentration falls below a critical value. It is therefore conceivable that as a result of condensation in the air-gap a thin solid crust is formed at the periphery of the fiber. This crust may be torn apart when the fiber enters the coagulation bath and this may be detrimental to the spinning process and hence to the features of the final product.

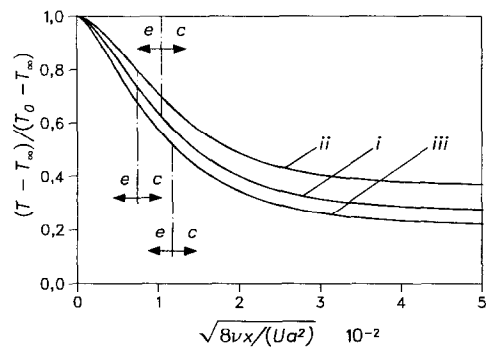

FIG. 6. Calculated temperature profiles for different initial temperatures T_0; cases (i)–(iii). In case (ii) $T_{0,ii} = T_{0,i} - 20$ K. In case (iii) $T_{0,iii} = T_{0,i} + 20$ K.

Acknowledgements—All experimental data were provided by Akzo Research Laboratories, Obernburg. I am indebted to Professor J. H. Spurk, who initiated this work, for his advice and helpful discussions. I have also greatly benefitted from valuable conversations with Dr. G. Frischmann. Many thanks go to Professor J. T. Jenkins for improvements of the English language of this paper.

REFERENCES

1. V. Simon, The mechanics of air-gap wet-spinning of fibers. In *Theoretical and Applied Rheology, Proc. XIth Int. Congr. on Rheology*, Brussels (Edited by P. Moldenaers und R. Keunings), pp. 391–393. Elsevier Science Publishers, Amsterdam (1992).
2. R. M. Griffith, Velocity, temperature, and concentration distribution during fibre spinning, *Ind. Engng Chem. Fundam.* **3**, 245–250 (1964).
3. D. E. Bourne and H. Dixon, The cooling of fibers in the

formation process, *Int. J. Heat Mass Transfer* **24,** 1323–1332 (1971).
4. H. K. Kuiken, The cooling of a low-heat-resistance cylinder moving through a fluid, *Proc. R. Soc. Lond.* **A346,** 23–35 (1975).
5. R. Münzing, Temperaturverteilung im Spinnfaden, Diplomarbeit, Fachgebiet Technische Strömungslehre, Technische Hochschule Darmstadt (1992).
6. D. R. Paul, Diffusion during the coagulation step of wet-spinning, *J. Appl. Polym. Sci.* **12,** 383–402 (1968).
7. H. K. Kuiken, The cooling of a low-heat-resistance sheet moving through a fluid, *Proc. R. Soc. Lond.* **A341,** 233–252 (1974).
8. J. H. Spurk, *Strömungslehre* (3rd Edn). Springer, Berlin (1993).
9. K. Stephan and F. Mayinger, *Thermodynamik*, Vol. 2. Springer, Berlin (1992).
10. R. C. Reid, J. M. Prausnitz and B. E. Poling, *The Properties of Gases and Liquids* (4th Edn). McGraw-Hill, New York (1988).
11. L. J. Crane, Boundary layer flow on a circular cylinder moving in a fluid at rest, *ZAMP.* **23,** 201–212 (1972).
12. H. J. Herring and G. L. Mellor, A computer program to calculate incompressible laminar and turbulent boundary layer development, NACA Report CR 1564 (1970).
13. V. Simon, Theoretische Untersuchung des Luftspalt-Naßspinnprozesses von Textilfasern, Doctoral Dissertation, Technische Hochschule Darmstadt (1993).